



Conjugated microporous polymers as a novel generation of drug carriers: A systemic study toward efficient carriers of tetracycline antibiotic

Aya Osama Mousa^{a,b}, Mohamed Gamal Mohamed^{a,c,*}, Zheng-Ian Lin^d, Cheng-Hsin Chuang^{b,*}, Chih-Kuang Chen^{d,*}, Shiao-Wei Kuo^{a,e,*}

^a Department of Materials and Optoelectronic Science, Center of Crystal Research, National Sun Yat-Sen University, Kaohsiung 804, Taiwan

^b Institute of Medical Science and Technology, College of Medicine, National Sun Yat-Sen University, Kaohsiung 804201, Taiwan

^c Chemistry Department, Faculty of Science, Assiut University, Assiut 71515, Egypt

^d Polymeric Biomaterials Laboratory, Department of Materials and Optoelectronic Science, National Sun Yat-Sen University, Kaohsiung 804, Taiwan

^e Department of Medicinal and Applied Chemistry, Kaohsiung Medical University, Kaohsiung 807, Taiwan

ARTICLE INFO

Keywords:

2,1,3-benzothiadiazole
Conjugated microporous polymers
Suzuki coupling
MTT assay
Drug carriers

ABSTRACT

Herein, a novel approach for synthesizing three distinct types of conjugated microporous polymers (CMPs) is presented. The method involves utilizing 2,1,3-benzothiadiazole (BBT) as a common monomeric unit, along with other monomeric units such as triphenylamine (TPA), tetraphenylethylene (TPE), and pyrene (Py), which exhibit varying levels of planarity. The synthesis of CMPs is achieved through a Suzuki coupling condensation reaction involving 4,7-dibromo-2,1,3-benzothiadiazole (BBT-Br₂) and 1,4-benzenboronic acid [PhB(OH)₂]. The resulting CMPs possess unique structural characteristics, adjustable pore sizes, and exceptional chemical and physical properties, thereby surpassing other existing materials in their performance. Notably, these CMPs demonstrate favorable thermal stability and porosity comparable to previously reported CMPs in the literature. Among the synthesized CMPs, the TPE-Ph-BBT CMP exhibits the highest thermal stability, with a char yield of 72 wt%. Additionally, the biocompatibility and toxicity of the CMPs are assessed using an MTT assay and a live/dead cell viability assay. The findings reveal that the CMPs exhibit low toxicity and outstanding biocompatibility, as evidenced by cell viability values exceeding 90% after 24 or 48 h of incubation. Thus, these CMPs hold significant potential for biomedical applications. Furthermore, the CMPs can effectively serve as drug carriers for tetracycline antibiotics. The antimicrobial activity of tetracycline (TCH)-loaded CMPs is evaluated using an inhibition zone methodology, demonstrating wide zones of inhibition measuring up to 1.7 cm against *Staphylococcus aureus* (*S. aureus*) and 1.9 cm against *Escherichia coli* (*E. coli*). This study highlights the promising prospects of CMPs in molecular engineering and their utility in diverse therapeutic applications as efficient drug carriers.

1. Introduction

Recent years have seen a lot of interest in porous organic polymers (POPs) because of their varied shapes and uses [1,2]. These materials are formed through covalent bonds between monomeric building blocks, that significantly increase chemical stability in a variety of organic liquids [3–5]. POPs encompass various family members, including conjugated microporous polymers (CMPs) [6,7], porous aromatic frameworks (PAFs) [8,9], covalent organic frameworks (COFs) [10–12], hyper-cross-

linked polymers (HCPs) [13,14], polymers of intrinsic microporosity (PIMs) [15,16], and covalent triazine polymers or frameworks (CTPs or CTFs) [17–19]. The covalently bonded networks of POPs find utility in a variety of uses, including biomedicine, optoelectronics, heterogeneous catalysis, sensing, gas storage, and separation, among others [20–26]. POPs, or porous organic polymers, offer promising opportunities for a number of biomedical uses because of their capacity for being synthesized on a large scale, compatibility with cell viability and penetration, and diverse structural properties [27–37]. For the development of POPs,

* Corresponding authors at: Department of Materials and Optoelectronic Science, Center of Crystal Research, National Sun Yat-Sen University, Kaohsiung 804, Taiwan (M.G. Mohamed and S.-W. Kuo).

E-mail addresses: mgamal.eldin12@yahoo.com (M.G. Mohamed), chchuang@imst.nsysu.edu.tw (C.-H. Chuang), chihkuan@mail.nsysu.edu.tw (C.-K. Chen), kuosw@faculty.nsysu.edu.tw (S.-W. Kuo).

<https://doi.org/10.1016/j.eurpolymj.2023.112254>

Received 8 May 2023; Received in revised form 12 June 2023; Accepted 20 June 2023

Available online 28 June 2023

0014-3057/© 2023 Elsevier Ltd. All rights reserved.

significant study endeavors have been made specifically for their potential biomedical applications. One key advantage of POPs over inorganic porous materials or MOFs is their construction from metal-free organic building blocks, which may result in lower cytotoxicity and improved biocompatibility, making them particularly appealing to use in biomedical fields. One of the many POPs, CMPs, or conjugated microporous polymers, have emerged as a particularly intriguing option for biomedical applications [38–40]. CMPs are typically synthesized through a sequence of polycondensation reactions, including methods such as Suzuki coupling, metathesis, Sonogashira coupling, oxidative polymerization, Buchwald-Hartwig Amination, and Knoevenagel reaction [41–46]. CMPs, or conjugated microporous polymers, are distinct from other porous polymers because of their expanded π -conjugated skeletons and intrinsic porosity, which create an extended conjugation structure in their backbone [47]. This unique structure makes CMPs highly useful in various biomedical applications, such as biosensing, bioimaging, drug delivery, antibacterial treatments, and phototherapy [48–54]. In addition, CMPs and their derivatives have attracted notice recently as promising adsorbents because of their exceptional structural characteristics [55,56]. Imteaz Ahmed et al. used a new mesoporous N-doped carbonaceous material with excellent sulfonamides adsorption properties [57]. Zhang et al. prepared diol-based porous organic polymers (POPs) with a permeable diol structure effectively combined with tetracycline (TC), and the results exhibited excellent TC removal efficiency [58]. POP materials, with their unique chemical structure that includes flexible linking groups between rigid aromatic rings, suitable functional group density, and graded porosity, offer potential as effective candidates for the removal of antibiotics. This is due to their efficient adsorption properties. Furthermore, CMPs can serve as carriers for loading antimicrobial agents such as antibiotics, antimicrobial peptides,

photosensitizers, etc. and releasing them from the CMPs structure to inhibit bacterial growth. Consequently, looking into inexpensive resources for effective antibiotic therapeutics is essential. Additionally, many medicines have disadvantages like poor stability, side effects, and toxicity. However, by selecting a suitable drug carrier, these disadvantages can be eliminated, making drug carriers an essential component in addressing these issues [59]. Our objective was to develop affordable antibiotic-loaded CMPs that can be manufactured in large quantities, to mitigate the toxicity associated with direct antibiotic use and augment their antimicrobial efficacy. In this study, we present three novel CMPs' preparation and characterization based on TPA/TPE/Py and BBT units through a Suzuki coupling condensation protocol, namely TPA-Ph-BBT, TPE-Ph-BBT, and Py-Ph-BBT CMPs, as depicted in Fig. 1. We used various techniques, including FTIR, SSNMR, TGA, XPS, BET, SEM, TEM, and PXRD, to emphasize their molecular structures, thermal robustness, porosities, morphologies, and amorphous natures. We also evaluated their nonhazardous nature using the MTT assay methodology. Furthermore, we demonstrated the use of these three new BBT-CMPs as drug carriers for the antibiotic tetracycline hydrochloride (TCH) by providing abundant coordination sites for π - π stacking with TCH through the structural aromatic rings of BBT-CMPs, enhancing the loading capacity of TCH, and providing effective anchoring of TCH in BBT-CMPs, avoiding self-aggregation of CMPs, and greatly enhancing the antibacterial activity. We evaluated the antimicrobial activity of these carriers using a zone of inhibition method. Overall, our study shows that these low-cost and mass-producible antibiotic-loaded CMPs have low toxicity, good biocompatibility, and enhanced antimicrobial impact compared to direct antimicrobial treatment, making them promising candidates for future drug delivery systems.

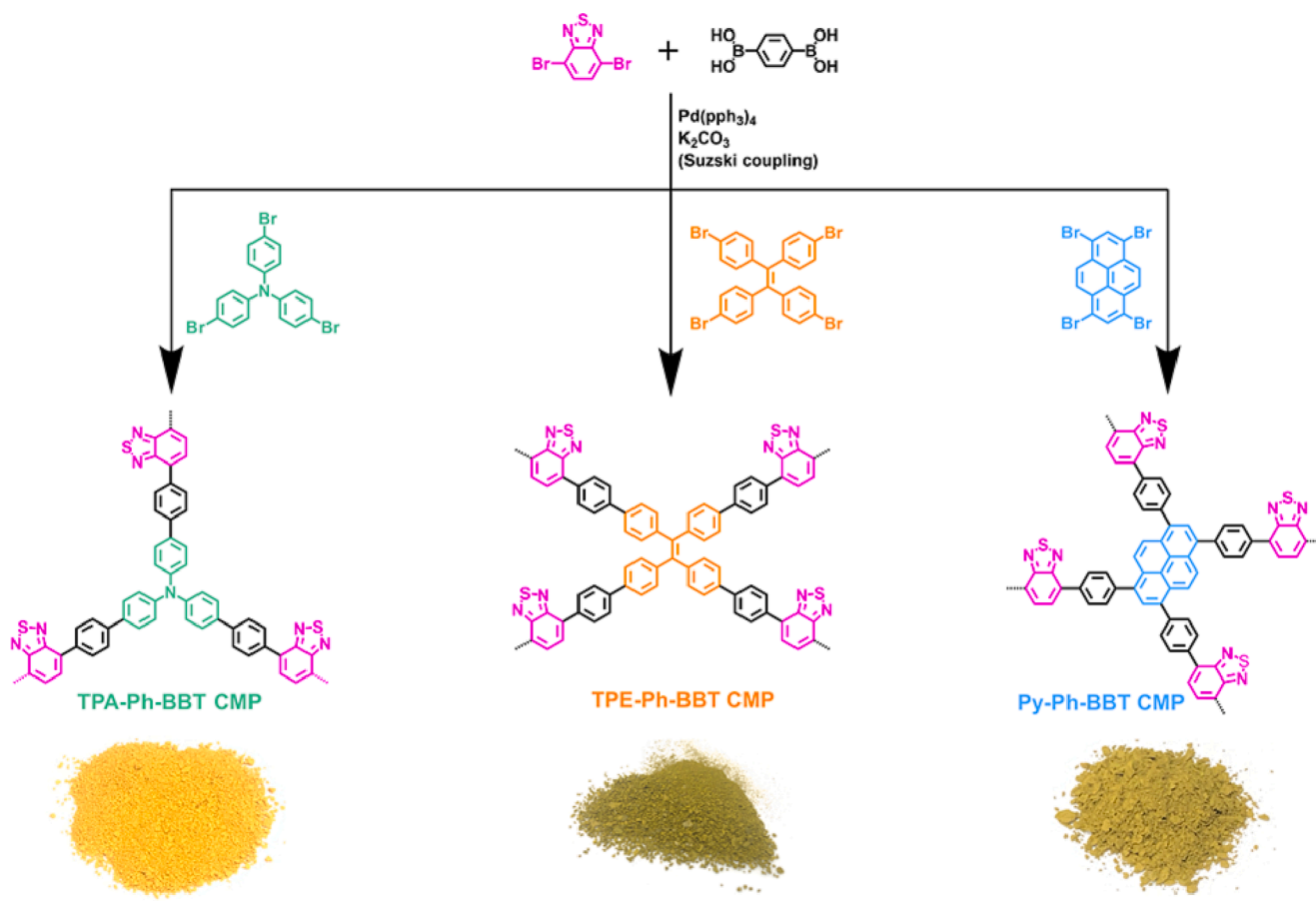


Fig. 1. Schematic representation of the preparation of (a) TPA-Ph-BBT, (b) TPE-Ph-BBT, and (c) Py-Ph-BBT CMPs.

2. Experimental section

2.1. Materials

Pyrene (Py, 98%), triphenylamine (TPA), bromine (Br₂), ethanol (EtOH), dichloromethane (DCM), acetic acid (AcOH), benzophenone (Benz, 99%), zinc (Zn, 98%), tetrahydrofuran (THF), titanium tetrachloride (TiCl₄, 99.9%), potassium carbonate (K₂CO₃, 99.9%), tetrakis(triphenylphosphine)palladium (Pd(PPh₃)₄), ethyl acetate (EA), methanol (MeOH), acetone and dimethylformamide (DMF) were purchased from J. T. Baker. nitrobenzene, anhydrous magnesium sulfate (MgSO₄, 99.5%), 1,4-benzenboronic acid [PhB(OH)₂], 2,1,3-benzothiadiazole (BBT), and N-bromosuccinimide (NBS, 99 %) were obtained from Acros. tetracycline hydrochloride (TCH, 98%) was purchased from Alfa Aesar without further purification.

2.2. Synthesis of 1,3,6,8-Tetrabromopyrene (Py-Br₄)

To synthesize Py-Br₄, a round flask with a single neck was used. A solution of bromine (4.6 mL, 88 mmol) was dissolved in 40 mL of nitrobenzene in a flask. Then, 4.00 g of pyrene was added to the solution, which was also dissolved in 40 mL of nitrobenzene. The resulting mixture was refluxed at 120 °C for four hours until a green powder was obtained. The green powder was washed repeatedly with ethanol, filtered, and dried to yield Py-Br₄ (Scheme S1, 8.80 g, 90%). FTIR (Figure S1): 3053 and 682 cm⁻¹. T_{d10} = 385 °C, measured by TGA under N₂.

2.3. Synthesis of tetraphenylethylene (TPE)

Zn (5.31 g, 81.2 mmol) and Benz (4.00 g, 21.8 mmol) were mixed in 100 mL of THF and agitated under nitrogen at ambient temperature for 10 min. The combination was then combined with TiCl₄ (4.60 mL, 42.17 mmol), and the resulting solution was refluxed at 80 °C for 24 h. Then, the combination was introduced to a 5% of K₂CO₃ solution, and the THF was evaporated under decreased pressure. EA was then used to separate the residual watery phase. To produce TPE (3.55 g, 97%) as a white solid, the EA was vaporized, and the obtained solid was then rinsed with ethanol.

as shown in Scheme S2. M.p.: 229 °C (Figure S2). FTIR (Figure S3): 3047. ¹H NMR (Figure S4): 7.15–7.08 (20H). ¹³C NMR (Figure S5): 140.70, 141.00, 131.30, 127.70, 126.4.

2.4. Synthesis of 1,1,2,2-Tetrakis(4-bromophenyl)ethene (TPE-Br₄)

TPE (6.64 g, 20 mmol) was dissolved in a solution of DCM (40 mL), and AcOH (20 mL), at 0 °C. The flask was then filled with Br₂ (8.00 mL, 160 mmol), and the resulting mixture was agitated at 0 °C for 48 h. After that, 400 mL of H₂O was added to the reaction, and DCM was used to separate the resulting TPE-Br₄ as a white powder. The yield of TPE-Br₄ was 12.3 g (95%), as shown in Scheme S2. M.p.: 262 °C (Figure S6). FTIR (Figure S7): 3051 and 1572 cm⁻¹. ¹H NMR (Figure S8): 7.25–6.84 (16H). ¹³C NMR (Figure S9): 142.30, 139.70, 133.70, 131.90, 121.80. T_{d10} = 354 °C, measured by TGA under N₂.

2.5. Synthesis of 4,7-dibromobenzo[*c*][1,2,5]thiadiazole (BBT-Br₂)

15 g (110.1 mmol) of BBT, 120 mL (48 % HBr), and a solution of 52.8 g (330.45 mmol) of Br₂ were all combined. The reaction was finished after the combination was elevated to reflux for 16 h at 100 °C. To isolate the product, the mixture was added to a cold NaOH solution and extracted with DCM. The resulting white powder of BBT-Br₂ weighed 7.5 g, which corresponds to a yield of 70% based on the starting amount of BBT. The synthesis of BBT-Br₂ is depicted in Scheme S3. FTIR (Figure S10): 3035. ¹H NMR (Figure S11): 7.73 (2H). ¹³C NMR (Figure S12): 154, 115.

2.6. Synthesis of Tris(4-bromophenyl)amine (TPA-Br₃)

2.00 g (11.5 mmol) of NBS was added to a round-bottom flask along with a solution of 0.918 g (3.74 mmol) of TPA in 30 mL of DMF. After that, the flask was agitated for 24 h at 0 °C. Following the vaporization of the DMF, the flask was filled with 600 mL of water and 400 mL of DCM. The organic component was condensed under pressure after being filtered and desiccated over MgSO₄. The resultant substance was repeatedly washed with MeOH to produce a white powder (1.88 g, 90%) as shown in Scheme S4. M.p.: 142 °C (Figure S13). FTIR (Figure S14): 3078, 1618 (CC stretching). ¹H NMR (Figure S15): 6.94–7.35 (12H). ¹³C NMR (Figure S16): 146.80–116.40. T_{d10} = 317 °C, measured by TGA under N₂.

2.7. Preparation of TPA-Ph-BBT, TPE-Ph-BBT and Py-Ph-BBT CMPs

To prepare TPA-Ph-BBT, TPE-Ph-BBT and Py-Ph-BBT CMPs a mixture of 0.4 g (0.83 mmol) of TPA-Br₃ or 0.48 g (0.76 mmol) of TPE-Br₄ or 0.5 g (0.97 mmol) of Py-Br₄, 0.2 g (1.21 mmol) of PhB(OH)₂, 0.12 g (0.41 mmol) of BBT-Br₂, 0.92 g (6.66 mmol) of K₂CO₃, and 0.05 g (0.04 mmol) of Pd(PPh₃)₄ in DMF (20 mL) and water (10 mL) under reflux for 72 h at 90 °C. After cooling, the substance was filtered off and successively rinsed with acetone, water, MeOH, and THF. The resulting orange solid was identified as TPA-Ph-BBT CMP, with a yield of 83%, as shown in Scheme S5, and green powder was identified as TPE-Ph-BBT CMP with a yield of 82%, as shown in Scheme S6 and Py-Ph-BBT CMP as a green solid with a yield of 75%, as depicted in Scheme S7.

2.8. Antibacterial test

In this experiment, the antimicrobial activity of TCH-TPA-Ph-BBT, TCH-TPE-Ph-BBT, and TCH-Py-Ph-BBT CMPs was tested using the modified Kirby-Bauer method. *S. aureus* (ATCC No. 25923) and *E. coli* (ATCC No. 25922) were used to serve as bacterial models. To prepare the bacterial solution, a UV-visible spectrophotometer (V-770, Jasco Inc.) was used to attain an optical density (OD) of 0.1 at 600 nm. The agar substrate was then inoculated with 100 μL of the bacterial solution, and disc-shaped samples were carefully placed on the agar substrate. The substrate was then incubated at 37 °C for 24 h to allow the colonies to grow over the entire agar substrate. Finally, images of the inhibition circles of the samples were taken with a camera, and Image-Pro Plus measured the inhibition circles of the samples, and the average value was recorded by repeating three samples.

3. Results and discussion

3.1. Synthesis and molecular characterization of BBT-Linked CMPs

Several compounds were synthesized and characterized in this study. Py-Br₄ was obtained as a green powder by refluxing Py with Br₂ in nitrobenzene (Scheme S1). The synthesis of TPE-Br₄ involved two stages. (Scheme S2): first, TPE was prepared by reacting benzophenone with zinc in the presence of THF and TiCl₄; second, TPE-Br₄ was synthesized as a white powder by reacting TPE with Br₂ in CH₂Cl₂. BBT-Br₂ was obtained by reacting BBT with Br₂/HBr in the presence of AcOH (Scheme S3). TPA-Br₃ was synthesized as a white powder by reacting TPA with NBS in the presence of DMF (Scheme S4). DSC, FTIR, and NMR analysis confirmed the purity of Py-Br₄, TPE, TPE-Br₄, and TPA-Br₃. The stretching vibrations of the C–H aromatic and C=C bonds, respectively, were ascribed to the bands at 3047 and 1602 cm⁻¹ in the FTIR spectrum of TPE [Figure S3]. The ¹H NMR spectrum of TPE [Figure S4] displayed proton signals for the aromatic rings at 7.14 and 7.04 ppm, while the ¹³C NMR profile of TPE indicated evidence for aromatic ring carbon atoms in the range of 144.06–126.56 ppm [Figure S5]. Py-Br₄, TPE-Br₄, and TPA-Br₃ also exhibited FTIR bands in the range of 3078–3047 and 1618–1572 cm⁻¹, corresponding to

vibrational modes of aryl C–H bond and C=C bonds [Figures S1, S7 and S14]. Other spectroscopic results of Py-Br₄, TPE-Br₄, BBT-Br₂, and TPA-Br₃ are discussed in detail in the experimental part and their characterization are provided in the supporting information file. The synthesis of three BBT-CMP was achieved through Suzuki polymerizations in DMF and H₂O mixtures with K₂CO₃ and Pd as the catalyst at 90 °C under a N₂ atmosphere, as shown in Fig. 1. TPA-Ph-BBT, TPE-Ph-BBT, and Py-Ph-BBT CMPs were obtained as orange [Fig. 1(a)], green [Fig. 1(b)], and green solids [Fig. 1(c)], respectively, from the reactions of TPA-Br₃, TPE-Br₄, and Py-Br₄ with PhB(OH)₂ and BBT-Br₂. The resultant BBT-CMPs showed porosity properties, as they weren't soluble in any of the examined liquids [DMF, MeOH, THF, DCM, acetone, and DMSO], indicating significant crosslinking densities and polymerization. FTIR and solid-state ¹³C NMR spectroscopy were used to corroborate the molecular structures of the produced BBT-CMPs. The FTIR spectra of the three BBT-CMPs [Fig. 2(a)], showed intense signals at 1604 cm⁻¹, indicating their imine (C=N) stretching. The absorption peaks at 1595 and 3098–3021 cm⁻¹ represented the C=C bonds and their C–H aromatic stretching vibrations. Also, in all BBT-CMPs, the signal corresponding to C–Br in the FTIR profiles was completely absent or undetectable [Figures S17–S19]. The solid-state ¹³C NMR analysis [Fig. 2(b)], showed carbon signals in the range of 143–116.7 ppm comparable to the phenyl groups and signal at 170 ppm representing C=N bonds. The thermal stabilities of BBT-CMPs were examined through TGA under N₂ atmospheres [Fig. 2(c)]. TPA-Ph-BBT, TPE-Ph-BBT, and Py-Ph-BBT CMPs showed thermal degradation temperatures T_{d5} and T_{d10} of 410 and 491 °C, 404 and 554 °C, and 341 and 357 °C, respectively. The TPA-Ph-BBT, TPE-Ph-BBT, and Py-Ph-BBT CMPs also displayed char yields of 71 wt%, 72 wt%, and 18 wt%, respectively.

Finally, the elemental compositions of the BBT CMPs were confirmed using XPS, which demonstrated the existence of S, C, and N elements in all three BBT-CMPs, as depicted in Fig. 2(d).

We conducted N₂ adsorption/desorption measurements to investigate the porosities of three BBT-CMP. The N₂ adsorption curves (Fig. 3 (a–c)) showed a rapid increase in N₂ uptake for values higher than 0.9 in all three BBT-CMPs. The presence of hysteresis in the desorption processes of the TPE-Ph-BBT CMPs revealed that the framework structure of this material possessed both mesoporous and microporous characteristics.

The N₂ isotherm profiles of all three BBT-CMPs were type III curves according to IUPAC nomenclature. The S_{BET} and total pore volumes for TPA-Ph-BBT CMP were 33.4 m² g⁻¹ and 0.214 cm³ g⁻¹, respectively. These values were followed by TPE-Ph-BBT CMP at 39.7 m² g⁻¹ and 0.26 cm³ g⁻¹, and Py-Ph-BBT CMP at 11.1 m² g⁻¹ and 0.085 cm³ g⁻¹, respectively. By using NLDFT, we estimated the pore sizes of TPA-Ph-BBT CMP to be 2.5 nm, TPE-Ph-BBT CMP to be 2.6 and 4.6 nm, and Py-Ph-BBT CMP to be 2.3 nm (Fig. 3(d–f)). This indicates that there is a microporous architecture in these BBT-CMP frameworks.

SEM and TEM techniques were utilized to investigate the morphologies of the produced BBT-CMPs. The as-synthesized BBT-CMPs exhibit varying morphologies, ranging from spherical to tubular structures, depending on their planarity degrees. SEM images [Fig. 4(a) and 4(b)] of TPA-Ph-BBT and TPE-Ph-BBT CMPs indicate their spherical shapes with some degree of aggregation, while the SEM image of Py-Ph-BBT CMP reveals a tube-like structure [Fig. 4(c)]. The tubular morphology of Py-Ph-BBT CMP can be attributed to the higher planarity of Py units, which enhances their assembly in this form [60,61]. The HR-TEM images revealed the existence of bright and alternating dark areas in TPA-

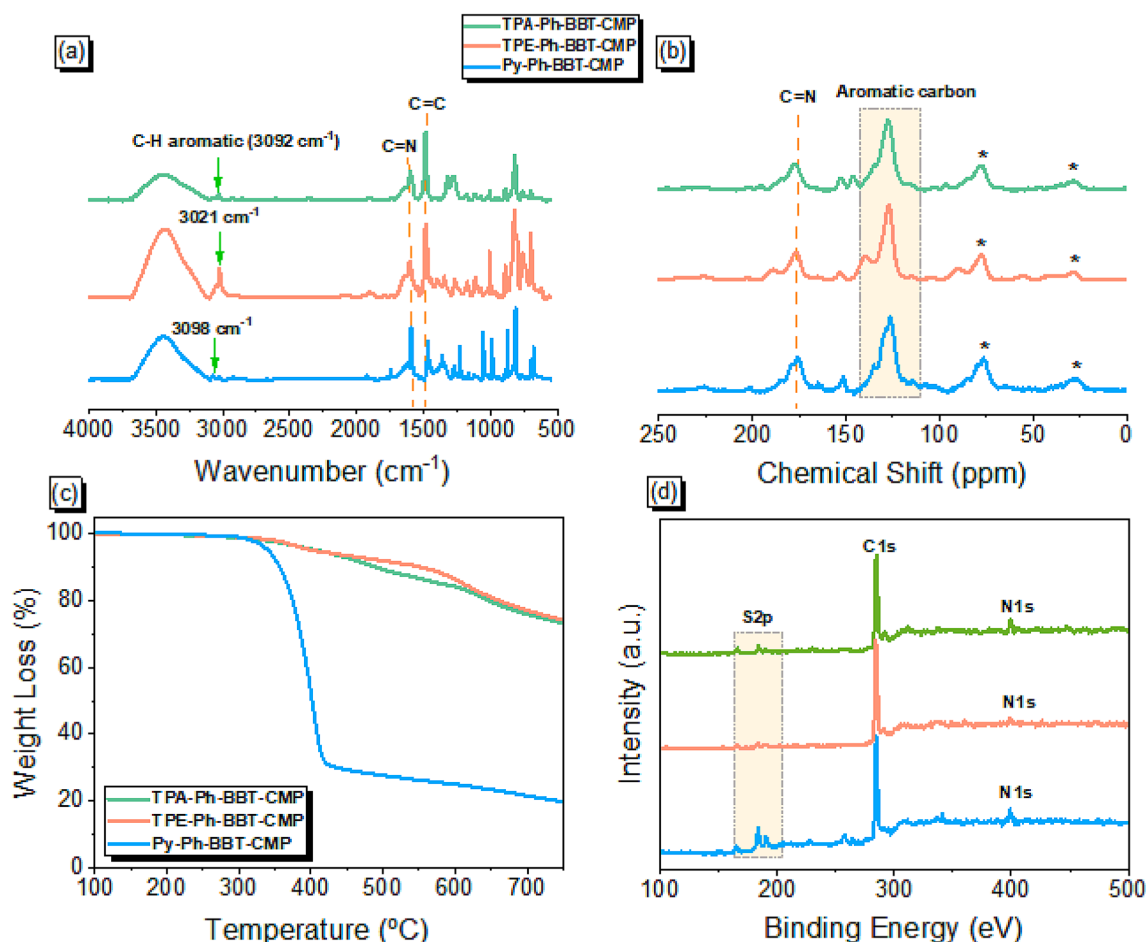


Fig. 2. (a) FTIR spectra, (b) solid-state NMR spectra, (c) TGA, and (d) XPS of TPA-Ph-BBT, TPE-Ph-BBT, and Py-Ph-BBT CMPs.

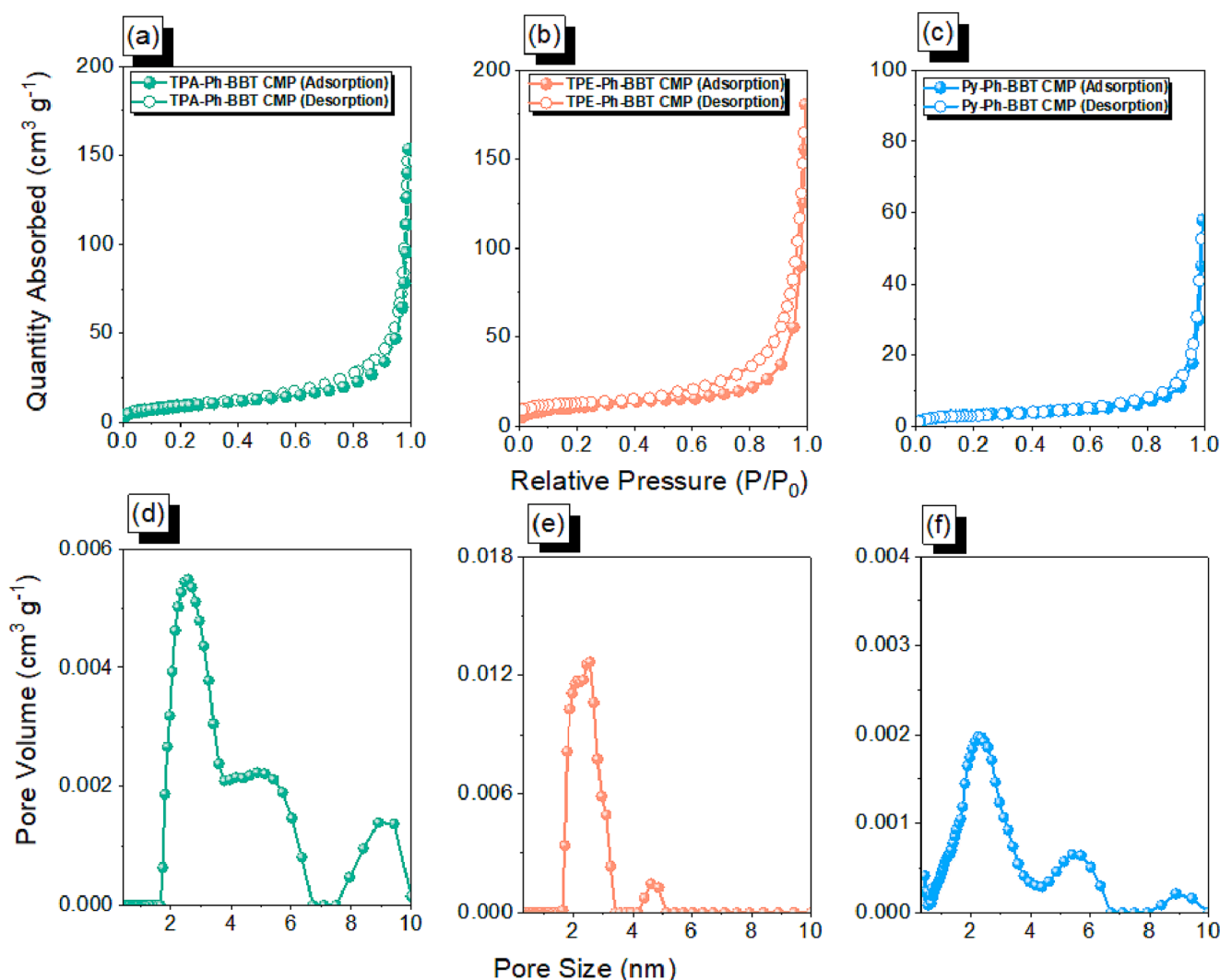


Fig. 3. (a – c) N_2 adsorption/desorption isotherms and (d – f) pore size distribution patterns of TPA-Ph-BBT (a and d), TPE-Ph-BBT (b and e), and Py-Ph-BBT CMPs (c and f).

Ph-BBT and TPE-Ph-BBT CMPs, indicating the presence of porous networks [Fig. 4(d) and 4(e)]. Similarly, the TEM image of Py-Ph-BBT CMP [Fig. 4(f)] showed a tube-like structure, consistent with the SEM images [60,61]. Additionally, elemental mapping of TPA-Ph-BBT, TPE-Ph-BBT, and Py-Ph-BBT CMPs based on SEM analysis revealed the existence of C, N, and S elements with homogeneous distributions on their surfaces [Figures S20, S21, and S22]. Figures S23-S25 revealed the amorphous nature of TPA-Ph-BBT and TPE-Ph-BBT CMPs through powder X-ray diffraction (PXRD), while Py-Ph-BBT CMP exhibited semicrystalline properties.

In Figure S26, the emission frequencies of TPA-Ph-BBT, TPE-Ph-BBT, and Py-Ph-BBT CMPs are observed at 619 nm, 550 nm, and 541 nm, respectively when tested in methanol solution. These emission wavelengths correspond to orange, yellow, and green colors, respectively. To ensure the safety of CMPs as drug carriers, it is important that they exhibit minimal toxicity. Thus, L929 mouse fibroblasts were utilized as test cells to assess their cytotoxicity. However, due to the insolubility of BBT-CMPs, the ISO 10993-5 standard screening technique was used to assess their cytotoxicity. The cell viability of TPA-Ph-BBT, TPE-Ph-BBT, and Py-Ph-BBT CMPs was evaluated after 24 and 48 h of incubation with L929 cells, as depicted in Fig. 5(a) and 5(b). The MTT assay results indicate that at CMP concentrations of 5, 10, and 20 mg/mL, the cell viability of L929 cells remained above 80% after both 24 and 48 h of incubation with the BBT-CMPs. This suggests that BBT-CMPs

exhibit minimal toxicity towards L929 cells, making them safe for use as functional drug carriers. Fig. 5(c) displays the results after 48 h of co-culture with L929 cells, demonstrating that the majority of cells in all CMP groups (TPA-Ph-BBT, TPE-Ph-BBT, and Py-Ph-BBT CMPs) remained viable and maintained a spindle-like morphology. These findings indicate that the BBT-CMPs possess minimal cytotoxicity. Notably, fluorescence microscopy revealed a yellow excitation from our CMPs, while the presence of CMPs did not adversely affect the viability of L929 cells. For the TCH-loaded CMPs study, representative Gram-positive bacteria (*S. aureus*) and Gram-negative bacteria (*E. coli*) were selected as test strains. To prepare TCH-TPA-Ph-BBT, TCH-TPE-Ph-BBT, and TCH-Py-Ph-BBT CMPs, a method was followed similar to that used for Py-Ph-BBT CMP. Initially, 20 mg of TCH and 20 mg of the respective CMPs were mixed in 5 mL of EtOH and sonicated in an ultrasonic water bath for 15 min until adsorption equilibrium was reached. The mixture was then subjected to centrifugation at 15000 rpm for 5 min to remove any unabsorbed TCH. Subsequently, the solvent was removed from TCH-TPA-Ph-BBT, TCH-TPE-Ph-BBT, and TCH-Py-Ph-BBT CMPs, respectively. When evaluating the drug loading amount, the TCH-TPA-Ph-BBT, TCH-TPE-Ph-BBT, and TCH-Py-Ph-BBT CMPs will be dispersed in deionized water, followed by ultrasonication for 30 min. Afterward, the dispersed solutions will be measured for absorbance at 360 nm. The loading content (LC) will be calculated based on the TCH-water calibration curve (Figure S27) and the following equations:

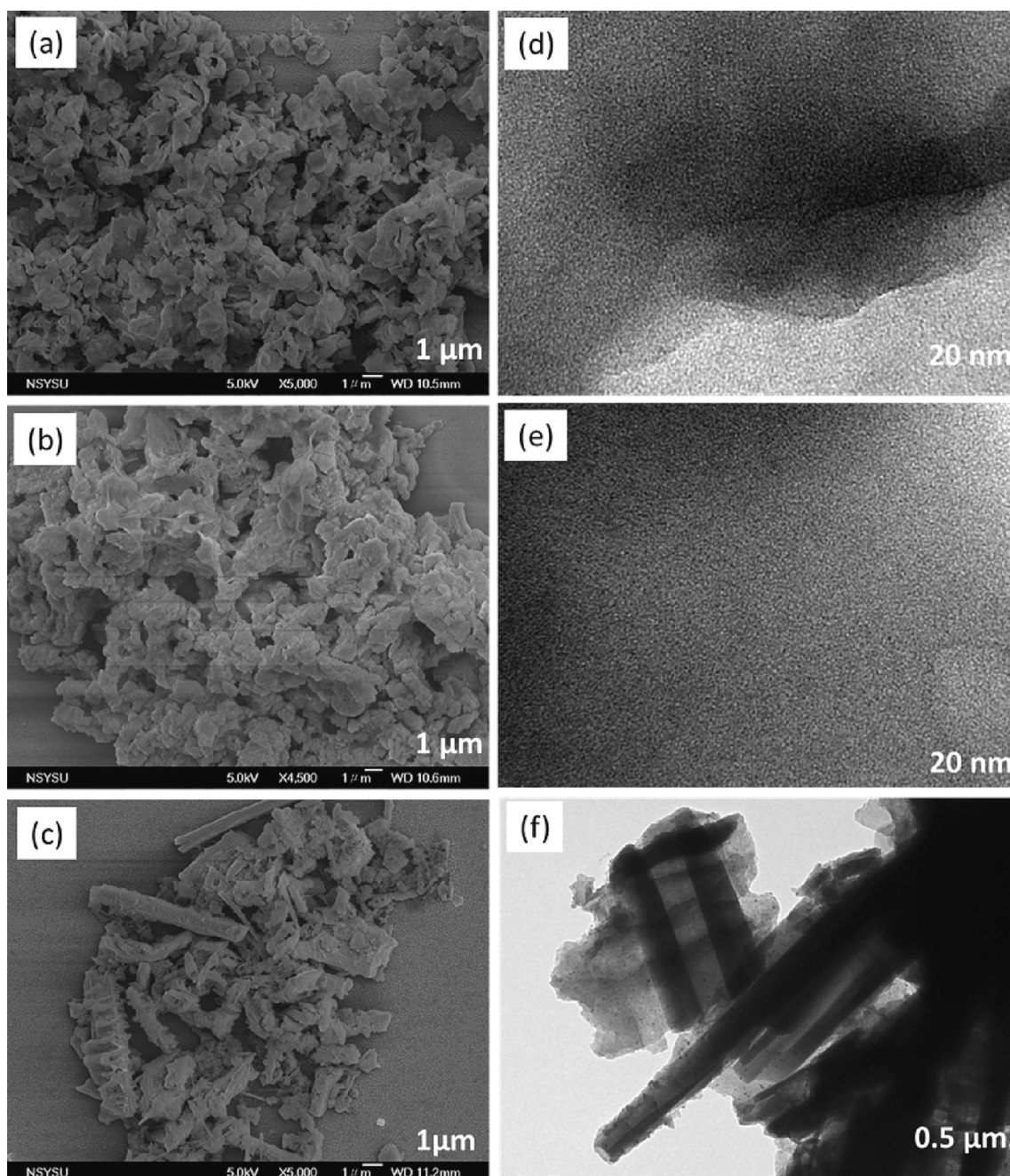


Fig. 4. SEM (a-c) and TEM (d-f) images of (a, d) TPA-Ph-BBT, (b, e) TPE-Ph-BBT, and (c, f) Py-Ph-BBT CMPs.

$$\text{LC (wt\%)} = (\text{weight of loaded TCH} / \text{weight of CMP}) \times 100 \%$$

The LC values for TCH-TPA-Ph-BBT, TCH-TPE-Ph-BBT, and TCH-Py-Ph-BBT CMPs are 3.0%, 0.7%, and 3.9%, respectively.

The resulting TCH-TPA-Ph-BBT, TCH-TPE-Ph-BBT, and TCH-Py-Ph-BBT CMPs were subsequently dried in an oven at 37 °C for 24 h. The filtered 6 mm filter paper was soaked in TCH-loaded CMPs suspension, air dried, and then adhered to agar plates with a predetermined amount of either *S. aureus* or *E. coli*. The plates were cultured at 37 °C for 24 h, and the diameter of the zone of inhibition produced by the test samples was recorded and compared. The results of the zone of inhibition test against *S. aureus* [Fig. 6(a)] showed that when BBT-CMPs were loaded with TCH, a clear zone of inhibition was observed. For example, TCH-TPE-Ph-BBT, TCH-Py-Ph-BBT, and TCH-TPA-Ph-BBT CMPs showed

zones of inhibition of 0.9 cm, 1.7 cm, and 1.4 cm, respectively. Fig. 6(b) illustrates the results obtained when testing the BBT-CMPs against *E. coli* bacteria. In this case, TCH-TPE-Ph-BBT, TCH-Py-Ph-BBT, and TCH-TPA-Ph-BBT CMPs exhibited inhibition zones measuring 0.7 cm, 1.7 cm, and 1.1 cm, respectively. These outcomes suggest that the release of TCH was effective in inhibiting the growth of *E. coli*. The higher antimicrobial efficiency of TCH-Py-Ph-BBT CMP compared to TCH-TPA-Ph-BBT CMP and TCH-TPE-Ph-BBT CMP indicates a higher TCH content of Py-Ph-BBT CMP due to the high planarity of the Py units, which facilitates π - π stacking between them, as illustrated in Fig. 7. The excellent antimicrobial performance observed in the study can be attributed to the release of TCH from the loaded CMPs, which effectively inhibits bacterial growth in the surrounding environment. Consequently, loading TCH onto CMPs enhances their antimicrobial activity. This study provides clear evidence that TCH-loaded CMP nanostructures exhibit

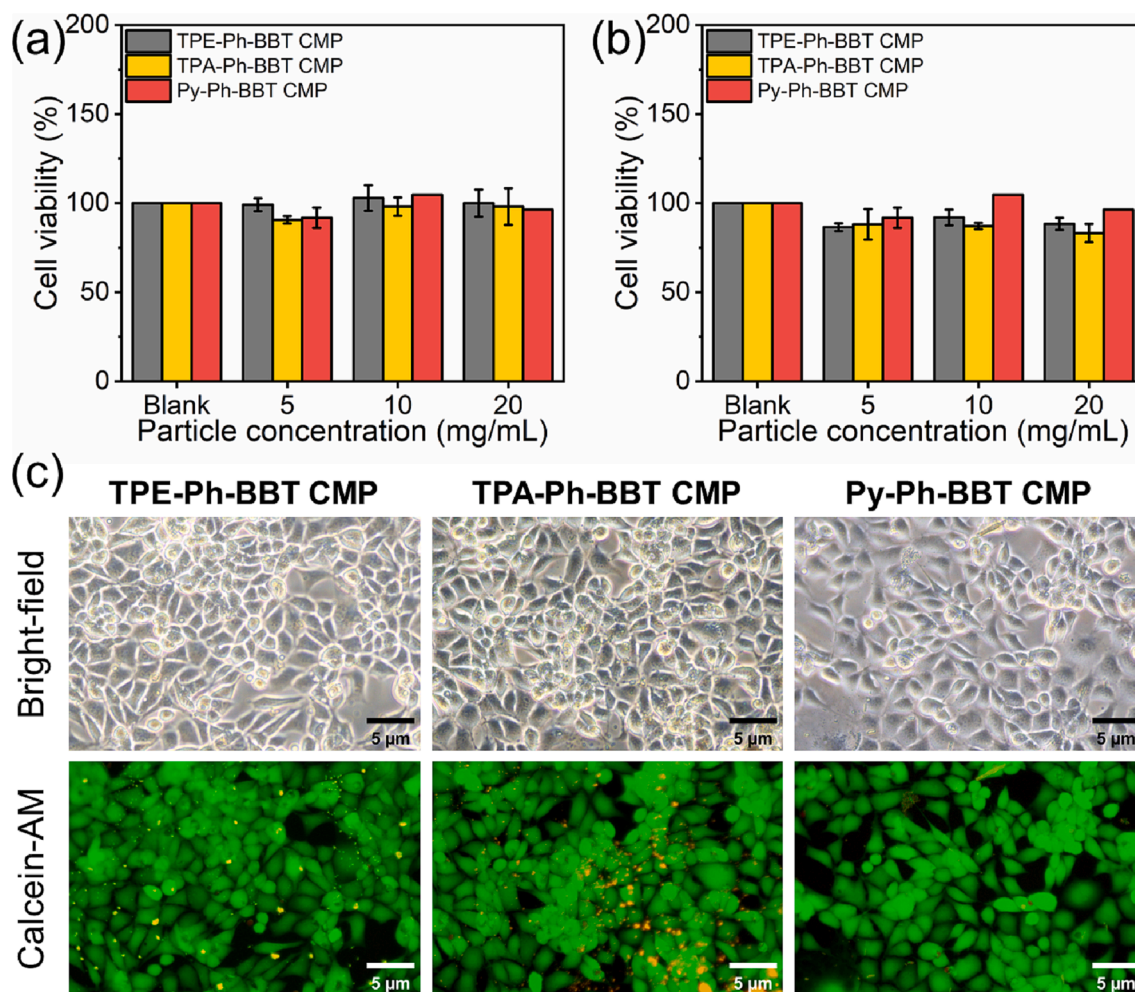


Fig. 5. Cytotoxicity assessment of TPE-Ph-BBT, TPA-Ph-BBT, and Py-Ph-BBT CMPs on L929 fibroblasts after (a) 24 h and (b) 48 h of culture (c) fluorescence images of L929 fibroblasts (Calcein-AM), after 48 h of culture.

antimicrobial activity. Furthermore, the antimicrobial effect of TCH primarily relies on the release of TCH from the TCH-loaded CMP nanostructures. TCH, a clinical antibiotic, can bind to the 16S rRNA of the bacterial ribosome's 30S subunit. Consequently, the released TCH effectively interferes with protein synthesis, thereby inhibiting bacterial growth. Based on these findings, the adsorption of TCH onto CMPs with porous structural characteristics, followed by the subsequent release of TCH from the TCH-loaded CMP nanostructures, proves to be an effective strategy for inhibiting bacterial growth.

Fig. 7 depicts the Py-Ph-BBT CMP, which contains Py moiety with numerous aromatic ring functional groups that can act as a π -electron acceptor. On the other hand, TCH has an aromatic ring structure and serves as a π -electron donor. The adsorption of TCH onto Py-Ph-BBT CMP is facilitated by the π - π interaction between the two molecules, aided by the porous nature of the CMP, which allows for pore filling. These factors collectively contribute to the adsorption of TCH onto Py-Ph-BBT CMP. Subsequently, upon exposure to both Gram-positive and Gram-negative bacteria, TCH is released from TCH-Py-Ph-BBT CMP, leading to the eradication of the bacteria and, thus, exhibiting an antibacterial effect.

4. Conclusion

We used the Suzuki coupling reaction to create three distinct CMPs based on the BBT moiety: TPA-Ph-BBT, TPE-Ph-BBT, and Py-Ph-BBT CMPs. These new BBT-CMPs were fully characterized and exhibited

tunable properties, such as thermal and porous features. For instance, TPE-Ph-BBT and TPA-Ph-BBT CMPs had T_{d10} at 554 and 491 °C, respectively, with a char yield of up to 71 wt%, as determined by TGA analysis. Furthermore, we assessed their cytotoxicity and biocompatibility in relation to L929 cells, revealing that they exhibited minimal toxicity and demonstrated high levels of biocompatibility. In addition, we used these CMPs as drug carriers for the antibiotic TCH and tested their antimicrobial activity against *S. aureus* and *E. coli* using the zone of inhibition method. Our results showed that TCH-TPE-Ph-BBT, TCH-Py-Ph-BBT, and TCH-TPA-Ph-BBT CMPs were effective in inhibiting the growth of *E. coli* and *S. aureus*. Notably, Py-Ph-BBT CMP, with its highly planar structure, exhibited the highest antimicrobial efficiency. Our study introduces a novel and significant approach to the utilization of a porous family of CMPs for biomedical applications via molecular engineering. This innovative strategy offers promising prospects for drug carriers, drug delivery systems, and bioimaging applications, presenting a range of potential candidates.

CRediT authorship contribution statement

Aya Osama Mousa: Investigation, Methodology. **Mohamed Gamal Mohamed:** Methodology, Conceptualization, Supervision, Writing – original draft. **Zheng-Ian Lin:** Investigation, Methodology. **Cheng-Hsin Chuang:** Supervision. **Chih-Kuang Chen:** Supervision. **Shiao-Wei Kuo:** Supervision.

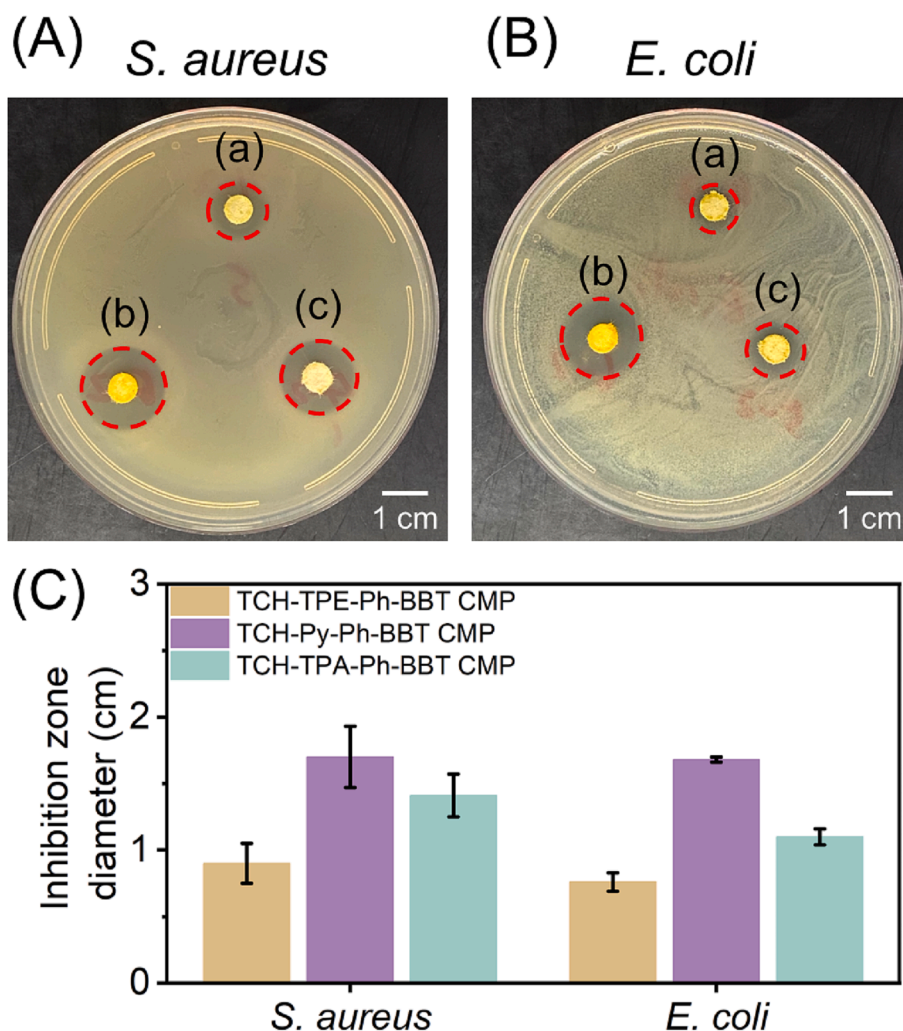


Fig. 6. Inhibition zone test results of (a) TCH-TPE-Ph-BBT CMP, (b) TCH-Py-Ph-BBT CMP, and (c) TCH-TPA-Ph-BBT CMP against (A) *S. aureus* and (B) *E. coli*, (C) the inhibition zone diameter ($n = 3$) for the TCH-loaded CMPs.

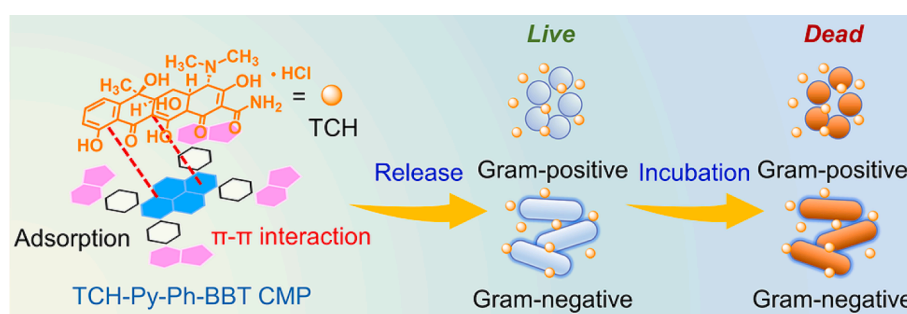


Fig. 7. Schematic representation of the π - π stacking between TCH and Py-Ph-BBT CMP to form TCH-loaded CMP for antibacterial application.

Declaration of Competing Interest

The authors declare that they have no known competing financial interests or personal relationships that could have appeared to influence the work reported in this paper.

Data availability

The data that has been used is confidential.

Acknowledgments

This study was supported financially by the Ministry of Science and Technology, Taiwan, under contracts NSTC 110-2124-M-002-013, 111-2223-E-110-004, NSTC 109-2221-E-110 -066 -MY3, and 110-2221-E-110 -001 -MY3. The authors thank the staff at National Sun Yat-sen University for their assistance with the TEM (ID: EM022600) experiments.

Appendix A. Supplementary material

Supplementary data to this article can be found online at <https://doi.org/10.1016/j.eurpolymj.2023.112254>.

References

- [1] M.G. Mohamed, A.F.M. EL-Mahdy, M.G. Kotp, S.W. Kuo, Advances in porous organic polymers: Syntheses, structures, and diverse applications. *Mater. Adv.* 3 (2022) 707–733. [10.1039/D1MA00771H](https://doi.org/10.1039/D1MA00771H).
- [2] J. Wang, L. Wang, Y. Wang, D. Zhang, Q. Xiao, J. Huang, Y.N. Liu, Recent progress in porous organic polymers and their application for CO₂ capture, *Chin. J. Chem. Eng.* 42 (2022) 91–103, <https://doi.org/10.1016/j.cjche.2021.08.028>.
- [3] M. Asad, M.I. Anwar, A. Abbas, A. Younas, S. Hussain, R. Gao, L.K. Li, M. Shahid, S. Khan, AIE based luminescent porous materials as cutting-edge tool for environmental monitoring: State of the art advances and perspectives, *Coord. Chem. Rev.* 463 (2022), 214539, <https://doi.org/10.1016/j.ccr.2022.214539>.
- [4] Z. Zhang, J. Jia, Y. Zhi, S. Ma, X. Liu, Porous organic polymers for light-driven organic transformations, *Chem. Soc. Rev.* 51 (2022) 2444–2490, <https://doi.org/10.1039/D1CS00808K>.
- [5] D.H. Yang, Y. Tao, X. Ding, B.H. Han, Porous organic polymers for electrocatalysis, *Chem. Soc. Rev.* 51 (2022) 761–791, <https://doi.org/10.1039/D1CS00887K>.
- [6] J.S.M. Lee, A.I. Cooper, Advances in conjugated microporous polymers, *Chem. Rev.* 120 (2020) 2171–2214, <https://doi.org/10.1021/acs.chemrev.9b00399>.
- [7] A. Hayat, M. Sohail, A. El Jery, K.M. Al-Zaydi, S. Raza, H. Ali, Y. Al-Hadeethi, T. Taha, I.U. Din, M.A. Khan, Recent advances in ground-breaking conjugated microporous polymers-based materials, their synthesis, modification and potential applications, *Mater. Today*. 64 (2023) 180–208, <https://doi.org/10.1016/j.mattod.2023.02.025>.
- [8] Y. Yuan, G. Zhu, Porous aromatic frameworks as a platform for multifunctional applications, *ACS central science* 5 (2019) 409–418, <https://doi.org/10.1021/acscentsci.9b00047>.
- [9] L. Căta, N. Terenti, C. Cociug, N.D. Hădăde, I. Grosu, C. Bucur, B. Cococaru, V.I. Parvulescu, M. Mazur, J.I. Cejka, Sonogashira Synthesis of New Porous Aromatic Framework-Entrapped Palladium Nanoparticles as Heterogeneous Catalysts for Suzuki–Miyaura Cross-Coupling, *ACS Appl. Mater. Interfaces* 14 (2022) 10428–10437. [10.1021/acsmi.1c24429](https://doi.org/10.1021/acsmi.1c24429).
- [10] M.G. Mohamed, E.C. Atayde Jr, B.M. Matsagar, J. Na, Y. Yamauchi, K.C.W. Wu, S. W. Kuo, Construction Hierarchically Mesoporous/Microporous Materials Based on Block Copolymer and Covalent Organic Framework, *J. Taiwan Inst. Chem. Eng.* 112 (2020) 180–192, <https://doi.org/10.1016/j.jtice.2020.06.013>.
- [11] A. Acharjya, P. Pachfule, J. Roeser, F.J. Schmitt, A. Thomas, Vinylene-linked covalent organic frameworks by base-catalyzed aldol condensation, *Angew. Chem. Int. Ed.* 58 (2019) 14865–14870, <https://doi.org/10.1002/anie.201905886>.
- [12] S. Liu, M. Wang, Y. He, Q. Cheng, T. Qian, C. Yan, Covalent organic frameworks towards photocatalytic applications: Design principles, achievements, and opportunities, *Coord. Chem. Rev.* 475 (2023), 214882, <https://doi.org/10.1016/j.ccr.2022.214882>.
- [13] J. Huang, S.R. Turner, Hypercrosslinked polymers: a review, *Polym. Rev.* 58 (2018) 1–41, <https://doi.org/10.1080/15583724.2017.1344703>.
- [14] M. Ejaz, M.G. Mohamed, W.C. Chang, S.W. Kuo, Synthesis and design of hypercrosslinked porous organic frameworks containing tetraphenylpyrazine unit for high-performance supercapacitor. *J. Polym. Sci.* (2023). <https://doi.org/10.1002/pol.20230174>.
- [15] N.B. McKeown, The synthesis of polymers of intrinsic microporosity (PIMs), *Sci. China Chem.* 60 (2017) 1023–1032, <https://doi.org/10.1007/s11426-017-9058-x>.
- [16] M.Z. Ahmad, R. Castro-Munoz, P.M. Budd, Boosting gas separation performance and suppressing the physical aging of polymers of intrinsic microporosity (PIM-1) by nanomaterial blending, *Nanoscale* 12 (2020) 23333–23370, <https://doi.org/10.1039/D0NR07042D>.
- [17] M.G. Mohamed, S.U. Sharma, N.Y. Liu, T.H. Mansoure, M.M. Samy, S.V. Chaganti, Y.L. Chang, J.T. Lee, S.W. Kuo, Ultrastable covalent triazine organic framework based on anthracene moiety as platform for high-performance carbon dioxide adsorption and supercapacitors. *Int. J. Mol. Sci.* 23 (2022) 3174. <https://doi.org/10.3390/ijms23063174>.
- [18] L. Liao, M. Li, Y. Yin, J. Chen, Q. Zhong, R. Du, S. Liu, Y. He, W. Fu, F. Zeng, Advances in the Synthesis of Covalent Triazine Frameworks, *ACS Omega* 8 (2023) 4527–4542, <https://doi.org/10.1021/acsomega.2c06961>.
- [19] S. Pourabrahimi, M. Pirooz, Functionalized covalent triazine frameworks as promising platforms for environmental remediation: A review, *Clean. Chem. Eng.* (2022), 100012, <https://doi.org/10.1016/j.cce.2022.100012>.
- [20] M.G. Mohamed, W.C. Chang, S.W. Kuo, Crown Ether- and Benzoxazine-Linked Porous Organic Polymers Displaying Enhanced Metal Ion and CO₂ Capture through Solid-State Chemical Transformation, *Macromolecules* 55 (2022) 7879–7892, <https://doi.org/10.1021/acs.macromol.1c00736>.
- [21] M.G. Mohamed, S.V. Chaganti, S.U. Sharma, M.M. Samy, M. Ejaz, J.T. Lee, K. Zhang, S.W. Kuo, Constructing Conjugated Microporous Polymers Containing the Pyrene-4, 5, 9, 10-Tetraone Unit for Energy Storage, *ACS Appl. Energy Mater.* 5 (2022) 10130–10140, <https://doi.org/10.1021/acsaem.2c01842>.
- [22] C. Weng, X. Li, Z. Yang, H. Long, C. Lu, L. Dong, S. Zhao, L. Tan, A directly linked COF-like conjugated microporous polymer based on naphthalene diimides for high performance supercapacitors, *Chem. Commun.* 58 (2022) 6809–6812, <https://doi.org/10.1039/D2CC02097A>.
- [23] Z. Li, Y.W. Yang, Macrocyclic-based porous organic polymers for separation, sensing, and catalysis, *Adv. Mater.* 34 (2022) 2107401, <https://doi.org/10.1002/adma.202107401>.
- [24] Q. Liu, Q. Sun, J. Shen, H. Li, Y. Zhang, W. Chen, S. Yu, X. Li, Y. Chen, Emerging tetrapyrrole porous organic polymers for chemosensing applications, *Coord. Chem. Rev.* 482 (2023), 215078, <https://doi.org/10.1016/j.ccr.2023.215078>.
- [25] Y.X. Zhang, The flexible EDAN-based covalent organic frameworks constructed by flexible knots and 4, 4'-ethylenedianiline as a linker for adsorbing and fluorescence sensing iodine, *Microporous Mesoporous Mater.* (2023), 112517, <https://doi.org/10.1016/j.micromeso.2023.112517>.
- [26] Z. Zhou, Y. Xiao, J. Tian, N. Nan, R. Song, J. Li, Recent advances in metal-free covalent organic frameworks for photocatalytic applications in energy and environmental fields, *J. Mater. Chem. A* 11 (2023) 3245–3261, <https://doi.org/10.1039/D2TA09582C>.
- [27] J.H. Kim, D.W. Kang, H. Yun, M. Kang, N. Singh, J.S. Kim, C.S. Hong, Post-synthetic modifications in porous organic polymers for biomedical and related applications, *Chem. Soc. Rev.* 51 (2022) 43–56, <https://doi.org/10.1039/D1CS00804H>.
- [28] S.K. Das, S. Mishra, K.D. Saha, D. Chandra, M. Hara, A.A. Mostafa, A. Bhaumik, N. Rich, Polyphenolic Porous Organic Polymer and Its In Vitro Anticancer Activity on Colorectal Cancer, *Molecules* 27 (2022) 7326, <https://doi.org/10.3390/molecules27217326>.
- [29] X. Jiao, F. Wu, A. Xie, L. Wu, W. Zhao, X. Zhu, X. Qi, Electrically conductive conjugate microporous polymers (CMPs) via confined polymerization of pyrrole for electromagnetic wave absorption, *Chem. Eng. J.* 398 (2020) 125591, <https://doi.org/10.1016/j.cej.2020.125591>.
- [30] A. Esrafil, A. Wagner, S. Inamdar, A.P. Acharya, Covalent organic frameworks for biomedical applications, *Adv. Healthc. Mater.* 10 (2021) 2002090, <https://doi.org/10.1002/adhm.2002090>.
- [31] N. Singh, S. Son, J. An, I. Kim, M. Choi, N. Kong, W. Tao, J.S. Kim, Nanoscale porous organic polymers for drug delivery and advanced cancer theranostics, *Chem. Soc. Rev.* 50 (2021) 12883–12896, <https://doi.org/10.1039/D1CS00559F>.
- [32] M. Li, Y. Zhang, X. Zhang, Z. Liu, J. Tang, M. Feng, B. Chen, D. Wu, J. Liu, Degradable Multifunctional Porphyrin-Based Porous Organic Polymer Nanosensitizer for Tumor-Specific Sonodynamic, Chemo- and Immunotherapy, *ACS Appl. Mater. Interfaces* 14 (2022) 48489–48501, <https://doi.org/10.1021/acsmi.2c14776>.
- [33] M. Hao, Y. Liu, W. Wu, S. Wang, X. Yang, Z. Chen, Z. Tang, Q. Huang, S. Wang, H. Yang, Advanced Porous Adsorbents for Radionuclides Elimination, *EnergyChem* (2023), 100101, <https://doi.org/10.1016/j.enchem.2023.100101>.
- [34] S. Bhunia, K.A. Deo, A.K. Gaharwar, 2D covalent organic frameworks for biomedical applications, *Adv. Funct. Mater.* 30 (2020) 2002046, <https://doi.org/10.1002/adfm.202002046>.
- [35] L. Feng, C. Qian, Y. Zhao, Recent advances in covalent organic framework-based nanosystems for bioimaging and therapeutic applications, *ACS Mater. Lett.* 2 (2020) 1074–1092, <https://doi.org/10.1021/acsmaterialslett.0c00260>.
- [36] X. Qi, Y. Xiang, E. Cai, S. You, T. Gao, Y. Lan, H. Deng, Z. Li, R. Hu, J. Shen, All-in-one: Harnessing multifunctional injectable natural hydrogels for ordered therapy of bacteria-infected diabetic wounds, *Chem. Eng. J.* 439 (2022), 135691, <https://doi.org/10.1016/j.cej.2022.135691>.
- [37] S. Wang, H. Li, H. Huang, X. Cao, X. Chen, D. Cao, Porous organic polymers as a platform for sensing applications, *Chem. Soc. Rev.* 51 (2022) 2031–2080, <https://doi.org/10.1039/D2CS00059H>.
- [38] M. Wang, S. Wang, X. Song, Z. Liang, X. Su, Photo-responsive oxidase mimic of conjugated microporous polymer for constructing a pH-sensitive fluorescent sensor for bio-enzyme sensing, *Sens. Actuators B Chem.* 316 (2020), 128157, <https://doi.org/10.1016/j.snb.2020.128157>.
- [39] W. Zhang, H. Zuo, Z. Cheng, Y. Shi, Z. Guo, N. Meng, A. Thomas, Y. Liao, Macroscopic conjugated microporous polymers: controlling versatile functionalities over several dimensions, *Adv. Mater.* 34 (2022) 2104952, <https://doi.org/10.1002/adma.202104952>.
- [40] X.X. Wang, L. Liu, Q.F. Li, H. Xiao, M.L. Wang, H.C. Tu, J.M. Lin, R.S. Zhao, Nitrogen-rich based conjugated microporous polymers for highly efficient adsorption and removal of COVID-19 antiviral drug chloroquine phosphate from environmental waters, *Sep. Purif. Technol.* 305 (2023), 122517, <https://doi.org/10.1016/j.seppur.2022.122517>.
- [41] T.H. Weng, M.G. Mohamed, S.U. Sharma, S.V. Chaganti, M.M. Samy, J.T. Lee, S. W. Kuo, Ultrastable three-dimensional triptycene- and tetraphenylethene-conjugated microporous polymers for energy storage, *ACS Appl. Energy Mater.* 5 (2022) 14239–14249, <https://doi.org/10.1021/acsaem.2c02809>.
- [42] M.G. Mohamed, H.Y. Hu, M. Madhu, M.M. Samy, I.M. Mekhemer, W.L. Tseng, H. H. Chou, S.W. Kuo, Ultrastable Two-Dimensional Fluorescent Conjugated Microporous Polymers Containing Pyrene and Fluorene Units for Metal Ion Sensing and Energy Storage, *Eur. Polym. J.* 139 (2023), 111980, <https://doi.org/10.1016/j.eurpolymj.2023.111980>.
- [43] A.O. Mousa, M.G. Mohamed, C.H. Chuang, S.W. Kuo, Carbonized Aminal-Linked Porous Organic Polymers Containing Pyrene and Triazine Units for Gas Uptake and Energy Storage, *Polymers* 15 (2023) 1891. <https://doi.org/10.3390/polym15081891>.
- [44] Y.S. Ye, M.G. Mohamed, C.W. Chen, S.W. Kuo, Integrating the multi-functionalities in metalloporphyrin porous organic polymers enabling strong polysulfide anchors and rapid electrochemical kinetics in Li-S battery, *J. Mater. Chem. A* 11 (2023) 9112–9124, <https://doi.org/10.1039/D2TA09232H>.
- [45] M.M. Samy, I.M.A. Mekhemer, M.G. Mohamed, M.H. Elsayed, K.H. Lin, Y.K. Chen, T.L. Wu, H.H. Chou, S.W. Kuo, Conjugated microporous polymers incorporating Thiazolo[5,4-d]thiazole moieties for Sunlight-Driven hydrogen production from

- water, *Chem. Eng. J.* 446 (2022), 137158, <https://doi.org/10.1016/j.cej.2022.137158>.
- [46] M.M. Samy, M.G. Mohamed, S.U. Sharma, S.V. Chaganti, T.H. Mansoure, J.T. Lee, T. Chen, S.W. Kuo, Constructing conjugated microporous polymers containing triphenylamine moieties for high-performance capacitive energy storage, *Polymer* 264 (2023), 125541, <https://doi.org/10.1016/j.polymer.2022.125541>.
- [47] A.O. Mousa, Z.I. Lin, C.H. Chuang, C.K. Chen, S.W. Kuo, M.G. Mohamed, Rational Design of Bifunctional Microporous Organic Polymers Containing Anthracene and Triphenylamine Units for Energy Storage and Biological Applications, *Int. J. Mol. Sci.* 24 (2023) 8966, <https://doi.org/10.3390/ijms24108966>.
- [48] Y. Zhu, P. Xu, X. Zhang, D. Wu, Emerging porous organic polymers for biomedical applications, *Chem. Soc. Rev.* 51 (2022) 1377–1414, <https://doi.org/10.1039/D1CS00871D>.
- [49] P. Palani, S. Karpagam, Conjugated polymers—a versatile platform for various photophysical, electrochemical and biomedical applications: a comprehensive review, *New J. Chem.* 45 (2021) 19182–19209, <https://doi.org/10.1039/D1NJ04062F>.
- [50] Y. Lei, Z. Zhu, H. Sun, P. Mu, W. Liang, A. Li, Conjugated microporous polymers bearing isocyanurate moiety as efficient antibacterial membrane and aerogels, *Sep. Purif. Technol.* 248 (2020), 117020, <https://doi.org/10.1016/j.seppur.2020.117020>.
- [51] Y. Wang, Q. Yuan, M. Li, Y. Tang, Y. Cationic Conjugated Microporous Polymers Coating for Dual-Modal Antimicrobial Inactivation with Self-Sterilization and Reusability Functions. *Adv. Funct. Mater.* (2023) 2213440. 10.1002/adfm.202213440.
- [52] S. Chen, H. Wang, X. Pan, C. Zhang, K. Zhang, Z. Chen, W. Dong, A. Xie, X. Qi, Dendritic Hydrogels with Robust Inherent Antibacterial Properties for Promoting Bacteria-Infected Wound Healing, *ACS Appl. Mater. Interfaces* 14 (2022) 11144–11155, <https://doi.org/10.1021/acscami.1c25014>.
- [53] Q. Xu, P. He, J. Wang, H. Chen, F.Lv, L. Liu, S.Wang, J. Yoon, J. Antimicrobial activity of a conjugated polymer with cationic backbone. *Dyes Pigm.* 160 (2019) 519–523. 10.1016/j.dyepig.2018.08.049.
- [54] H. Sun, W. Chan, S. Chen, H. Zhang, C. Ma, Z. Zhu, W. Liang, A. Li, Tissue paper-like conjugated microporous polymers film for bacteria inhibition, *J. Environ. Chem. Eng.* 10 (2022), 108933, <https://doi.org/10.1016/j.jece.2022.108933>.
- [55] X. Sheng, H. Shi, L. Yang, P. Shao, K. Yu, X. Luo, Rationally designed conjugated microporous polymers for contaminants adsorption, *Sci. Total Environ.* 750 (2021), 141683, <https://doi.org/10.1016/j.scitotenv.2020.141683>.
- [56] S. Wang, Q. Hu, Y. Liu, X. Meng, Y. Ye, X. Liu, X. Song, Z. Liang, Multifunctional conjugated microporous polymers with pyridine unit for efficient iodine sequestration, exceptional tetracycline sensing and removal, *J. Hazard. Mater.* 387 (2020), 121949, <https://doi.org/10.1016/j.jhazmat.2019.121949>.
- [57] I. Ahmed, H.J. Lee, S.H. Jhung, Covalent-organic polymer-derived carbons: An effective adsorbent to remove sulfonamide antibiotics from water, *Chem. Eng. J.* 437 (2022), 135386, <https://doi.org/10.1016/j.cej.2022.135386>.
- [58] S. Zhang, Y. Li, C. Shi, F. Guo, C. He, Z. Cao, J. Hu, C. Cui, H. Liu, Induced-fit adsorption of diol-based porous organic polymers for tetracycline removal, *Chemosphere* 212 (2018) 937–945, <https://doi.org/10.1016/j.chemosphere.2018.09.003>.
- [59] M.T. Taghizadeh, H. Ashassi-Sorkhabi, R. Afkari, A. Kazempour, Cross-linked chitosan in nano and bead scales as drug carriers for betamethasone and tetracycline. *Int. J. Biol. Macromol.* 131 (2019) 581–588. /10.1016/j.ijbiomac.2019.03.094.
- [60] G. Das, T. Skorjanc, S.K. Sharma, T. Prakasam, C. PlatasIglesias, D.S. Han, J. Raya, J.C. Olsen, R. Jagannathan, A. Trabolsi, Morphological diversity in nanoporous covalent organic materials derived from viologen and pyrene, *ChemNanoMat.* 4 (2018) 61–65, <https://doi.org/10.1002/cnma.201700242>.
- [61] X. Dong, F. Zhang, F. Huang, X. Lang, Pyrene-based conjugated microporous polymers for red light-powered oxidation of amines to imines, *Appl. Catal. B: Environ.* 318 (2022), 121875, <https://doi.org/10.1016/j.apcatb.2022.121875>.